© 2016. Published by The Company of Biologists Ltd | Journal of Experimental Biology (2016) 219, 2182-2191 doi:10.1242/jeb.140475

RESEARCH ARTICLE

Refuging rainbow trout selectively exploit flows behind tandem cylinders

William J. Stewart[1], Fang-bao Tian[2], Otar Akanyeti[1], Christina J. Walker[1] and James C. Liao[1,*]

ABSTRACT

Fishes may exploit environmental vortices to save in the cost of locomotion. Previous work has investigated fish refuging behind a single cylinder in current, a behavior termed the Kármán gait. However, current-swept habitats often contain aggregations of physical objects, and it is unclear how the complex hydrodynamics shed from multiple structures affect refuging in fish. To begin to address this, we investigated how the flow fields produced by two D-shaped cylinders arranged in tandem affect the ability of rainbow trout (*Oncorhynchus mykiss*) to Kármán gait. We altered the spacing of the two cylinders from *l*/*D* of 0.7 to 2.7 (where *l*=downstream spacing of cylinders and *D*=cylinder diameter) and recorded the kinematics of trout swimming behind the cylinders with high-speed video at *Re*=10,000–55,000. Digital particle image velocimetry showed that increasing *l*/*D* decreased the strength of the vortex street by an average of 53% and decreased the frequency that vortices were shed by ~20% for all speeds. Trout were able to Kármán gait behind all cylinder treatments despite these differences in the downstream wake; however, they Kármán gaited over twice as often behind closely spaced cylinders (*l*/*D*=0.7, 1.1, and 1.5). Computational fluid dynamics simulations show that when cylinders are widely spaced, the upstream cylinder generates a vortex street that interacts destructively with the downstream cylinder, producing weaker, more widely spaced and less-organized vortices that discourage Kármán gaiting. These findings are poised to help predict when fish may seek refuge in natural habitats based on the position and arrangement of stationary objects.

KEY WORDS: Vortex street, *Oncorhynchus mykiss*, Kármán gait, Flow visualization, DPIV, CFD, Turbulence, Swimming

INTRODUCTION

Fishes in current-swept environments must successfully navigate complex flows while performing tasks that are essential for survival, such as foraging for prey and evading predators. Turbulent flows have been shown to increase the cost of locomotion, probably because of the increased costs of stability (Webb, 1998; Enders et al., 2003). However, under certain situations, fish can exploit the energy of vortices in order to save energy during swimming (Liao et al., 2003a,b; Liao, 2004; Taguchi and Liao, 2011). For example, water flowing past a stationary cylinder generates rows of counter-rotating vortices that are alternately shed into the wake, known as a Kármán vortex street (Blevins, 1990). Fish refuging behind the cylinder adopt a unique swimming style called the Kármán gait, in which the body interacts with vortices to generate lift forces that propel the animal upstream (Liao et al., 2003a). The Kármán gait is visually distinct from steady swimming because the body exhibits much larger amplitude lateral motions that occur at a low frequency (Liao et al., 2003a,b; Akanyeti and Liao, 2013a,b). The Kármán gait offers almost 50% energy savings for the fish as it reduces the muscle activity and oxygen consumption required to swim against a current (Liao, 2004; Taguchi and Liao, 2011).

While fish readily refuge behind a single cylinder, a mechanistic understanding of how fish relate to the hydrodynamics around more complex structural arrangements found in nature, such as submerged branches, corals and mangrove roots, remains unexplored. To initiate a better understanding of how fish refuge in more complex hydrodynamic environments, we characterized the interaction between fish and the wake behind two cylinders, where one is positioned upstream of the other. We systematically changed the cylinder spacing and evaluated how the resultant wakes affect the ability of trout to Kármán gait.

For *Re* >100, tandem cylinders in flow shed vortices in patterns that are different from a single cylinder. Specifically, the patterns of vortex shedding around tandem cylinders can be classified into three distinct categories (Igarashi, 1981; Xu and Zhou, 2004; Sumner, 2010). (1) The extended body regime occurs when two closely-spaced cylinders behave hydrodynamically as a single bluff body. (2) The reattachment regime occurs at intermediate spacings and is characterized by the shear layer of the upstream cylinder reattaching to the downstream cylinder, resulting in attached vortices becoming established in the gap between the cylinders. (3) The co-shedding regime occurs when a wide spacing permits both cylinders to shed vortices, which then interact to form the downstream wake. Important characteristics of the vortex wake change across these three flow regimes, such as the frequency with which vortices are shed and the Strouhal number of the cylinders (Igarashi, 1981; Sumner, 2010). Characterizing these flow parameters is the first step to understanding the mechanisms that affect the refuging behavior of fishes behind multiple objects.

Our goals were to determine how cylinder spacing and flow speed affect the downstream wake and the ability of trout to hold station in this region. We recorded the kinematics of trout holding station behind tandem cylinders arrangements and separately quantified the flow using computational and experimental methods (Fig. 1). By demonstrating under what conditions trout are able to refuge behind aggregations of structures in flow, this work promotes the integration of more field-like environments into laboratory studies.

MATERIALS AND METHODS

Animals

Rainbow trout (*Oncorhynchus mykiss* Walbaum 1792) were obtained from the Chattahoochee Forest National Fish Hatchery, Suches, GA, USA. Fish were housed in a 473 liter circular tank

[1]Department of Biology, Whitney Laboratory for Marine Bioscience, University of Florida, St Augustine, FL 32080, USA. [2]School of Engineering and Information Technology, University of New South Wales, Canberra, Australian Capital Territory 2610, Australia.

*Author for correspondence (jliao@whitney.ufl.edu)

J.C.L., 0000-0003-0181-6995

Received 16 March 2016; Accepted 4 May 2016

Journal of Experimental Biology

Journal of Experimental Biology (2016) 219, 2182-2191 doi:10.1242/jeb.140475

List of symbols and abbreviations

D	diameter of cylinder
DPIV	digital particle image velocimetry
l	distance between cylinders
L_b	body length
$\mathbf{U}$	flow velocity (m s^{-1})
$\mathbf{U_f}$	nominal flow velocity upstream of the cylinder
$\bar{\mathbf{U}}_x$	time-averaged downstream velocity
VSF	vortex shedding frequency
VSF_{exp}	expected vortex shedding frequency
W	width of the working section of the flume

containing freshwater that was chilled to 15±1°C (Delta Star chiller, model DS-4-TXV, Aqua Logic, San Diego, CA, USA). Fish were fed commercial trout pellets daily and were maintained on a 12 h:12 h light:dark cycle. Four trout (total body length, L_b=18.9±0.52 cm) were used in the study.

Measuring Kármán gait kinematics

We collected high-speed video recordings of trout holding station behind tandem cylinders to evaluate how different arrangements of cylinders affected Kármán gaiting. Prior to experiments, trout were placed into a 175 liter re-circulating flow tank (25 cm height×26 cm width×87 cm length; Loligo Systems, Tjele, Denmark) and allowed to acclimate for 1 h at low flow velocity (2.5 L_b s^{-1}). Tandem D-shaped cylinders (5 cm diameter) were then secured vertically in the working section and the behavior of the fish was evaluated across six flow speeds (1–6 L_b s^{-1}) and six arrangements of cylinders (l/D=0.7, 1.1, 1.5, 1.9, 2.3, 2.7). Our selection of experimental flow speeds was motivated by measurements of what trout naturally experience (McLaughlin and Noakes, 1998; Liao, 2007). An experiment began once the fish initiated station holding behind the downstream cylinder. We observed swimming for 10 min and recorded all tail-beats from Kármán-gaiting fish with a high-speed camera (1000 fps, 1280×800 pixels, Phantom v.12.1, Vision Research, Wayne, NJ, USA).

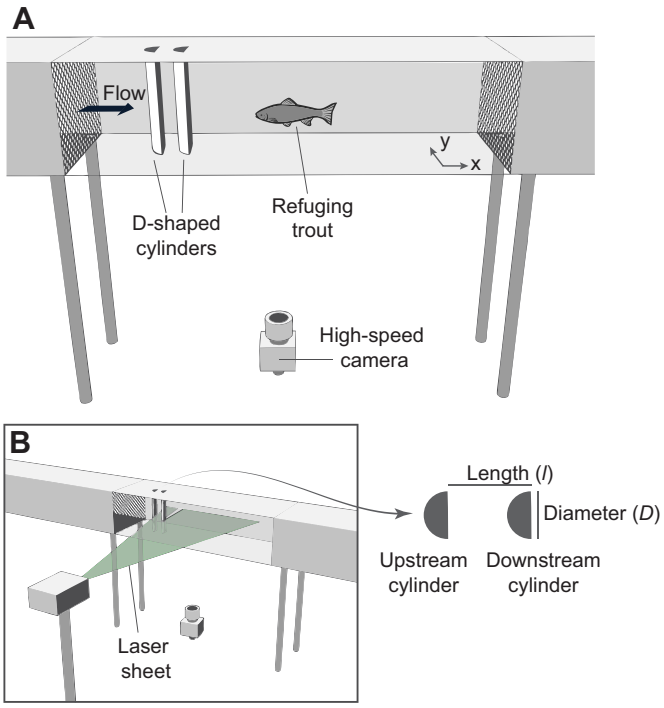

Fig. 1. Measuring the hydrodynamics and kinematics of trout refuging behind tandem cylinders. (A) Experimental setup illustrates the position of a high-speed camera used to record motions of trout refuging behind cylinders in a variable speed flow tank. (B) Light-reflective particles seeded in the flow tank were illuminated with a laser light sheet for digital particle image velocimetry (DPIV) to visualize and quantify the wake behind both upstream and downstream cylinders. Imaging of fish kinematics and the cylinder wake occurred in separate experiments so the DPIV laser did not interfere with the behavior of fish. The spacing between cylinders (l) was varied and normalized to the cylinder diameter (D).

Analysis of Kármán gait kinematics

We first identified video sequences when the fish were Kármán gaiting based on established criteria (Akanyeti and Liao, 2013a,b). Briefly, fish were required to (1) hold station with no upstream motion, (2) have a traveling wave along the body, (3) exhibit a lateral body displacement greater than ½ L_b, (4) possess a body wavelength longer than 1 L_b, and (5) exhibit no high-frequency tail beats. We used a custom script written in MATLAB (v.2012b, MathWorks, Natick, MA, USA) to digitize and analyze the body kinematics.

We compared Kármán-gaiting kinematics across cylinder treatments to evaluate the impact of flow speed and cylinder spacing. We calculated tail-beat frequency, body wavelength, the maximum lateral amplitude of four body locations (snout, center of mass, 50% L_b and tail) and downstream position (stream-wise distance from edge of the downstream cylinder to the fish snout). The center of mass was measured for anesthetized trout (0.0654 g l^{-1} tricaine methanesulfonate; MS-222, Argent Chemical Laboratories, Redmond, WA, USA) by iteratively balancing the body between right and left side pins. All kinematic parameters were compared across our treatments using linear regression in MATLAB. We defined the preference of fish to Kármán gait by the frequency of Kármán-gaiting tail-beats observed.

Quantifying the cylinder wake

To better understand how the different flow fields produced by our cylinder arrangements affect Kármán gaiting in trout, we used digital particle image velocimetry (DPIV) to quantify the vortex wakes. A horizontal laser sheet (25×15×0.1 cm) was generated with a 5 W, continuous argon ion laser (wavelength=532 nm, LaVision, Göttingen, Germany). The flow was seeded with neutrally buoyant, light-reflective particles (diameter, ~14 µm; Potters Industries, Valley Forge, PA, USA) that were illuminated by the laser sheet. A high-speed camera (Phantom Miro M310, Vision Research, Wayne, NJ, USA) positioned underneath the working section captured images (1280×800 pixels) of the particle field directly behind the downstream cylinder. DPIV recordings were conducted separately from live fish experiments so the laser did not affect the swimming behavior of fish.

Flow fields were visualized behind the same cylinder arrangements and flow speeds as our live fish experiments. For comparison, we also quantified the flow field behind a single cylinder. For each treatment, we recorded 20 continuously shed vortices behind the trailing cylinder. The frequency that vortices are expected to be shed from the trailing cylinder can be predicted according to the equation:

$$VSF_{exp} = St \times \mathbf{U} \times D^{-1}, \quad (1)$$

where VSF_{exp} is the expected vortex shedding frequency (Hz), St is the dimensionless Strouhal number (0.2 for cylinders, as in Liao et al., 2003a), $\mathbf{U}$ is the nominal flow speed (m s^{-1}) and D is the

Journal of Experimental Biology (2016) 219, 2182-2191 doi:10.1242/jeb.140475

cylinder diameter (m). We adjusted our video frame rate for DPIV analysis based on the expected VSF so that each vortex was imaged with approximately 200 video frames, resulting in video durations of 4000 frames for each treatment. These changes in frame rate for video also ensured that the displacements of DPIV particles between frames were appropriate for DPIV analysis.

The velocity fields of the cylinder wake were quantified from our DPIV recordings using DaVis software (v.8.1, LaVision). Each video image was divided equally into a 20×12 grid of windows that were each 64×64 pixels in size. Cross-correlation was performed on corresponding windows of sequential images to determine the average particle displacements between images for all windows in the grid. To improve the spatial resolution of our measurements, we performed a second cross-correlation routine on a finer window grid (32×32 pixels) with a 50% overlap, followed by a 3×3 smoothing spline of the resultant velocity vector fields. This analysis yielded 4000 sequential 80×50 velocity vector fields for each experimental treatment.

We computed time-averaged velocity vector fields for each treatment to compare the global flow fields produced by the different arrangements of cylinders and flow speeds. We measured the time-averaged downstream velocity field ($\bar{\mathbf{U}}_x$) to investigate how the spacing of cylinders affected the velocity deficit in the downstream wake. This was calculated as the mean of the horizontal component of each velocity vector ($\mathbf{U}_x$) through time. The temporal variation in the flow field was calculated as the standard deviation of the lateral component of each velocity vector ($\mathbf{U}_y$) over time.

Flow field analysis

We quantified the flow field behind different cylinder arrangements to better understand how the wake was related to Kármán gaiting. We analyzed the periodic characteristics of the flow by performing a fast Fourier transform of $\mathbf{U}_y$ versus time to reveal the frequency–power spectrum for all locations of the flow field. This analysis was restricted to frequencies less than 40 Hz due to the low-frequency

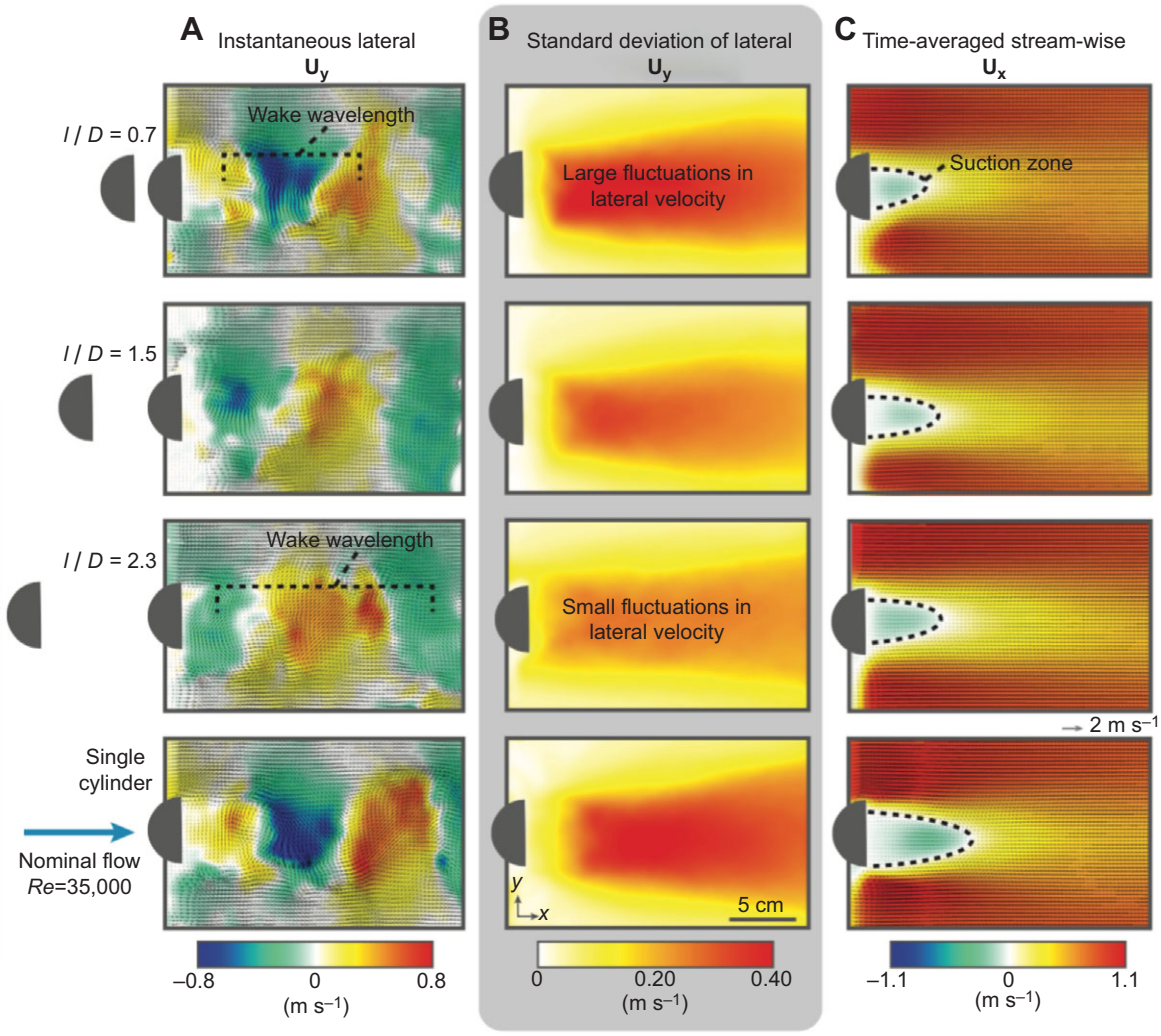

Fig. 2. Effect of cylinder spacing on rectilinear flow characteristics of the downstream wake. Flow characteristics behind tandem cylinders for a representative flow speed (0.7 m s^{-1}). The position of the downstream cylinder is shown for each panel, with the single-cylinder situation shown in the bottom row as a reference. (A) Magnitude of the instantaneous lateral flow velocity ($\mathbf{U}_y$) is color-coded for direction, with superimposed velocity vector fields (gray arrows) showing the speed and direction of overall flow. Higher lateral velocities are associated with more intense colors. (B) The standard deviation of $\mathbf{U}_y$ over time, where hotter colors indicate large fluctuations in the lateral flow velocity. (C) The suction zone behind the trailing cylinder of a tandem cylinder arrangement occupies a smaller area relative to a single cylinder, as revealed by the time-averaged and stream-wise component of flow velocity ($\mathbf{U}_x$). Red indicates downstream flow while blue indicates upstream flow.

Journal of Experimental Biology

Journal of Experimental Biology (2016) 219, 2182-2191 doi:10.1242/jeb.140475

characteristics expected for the shedding of vortices (Sumner, 2010). The peaks in the frequency–power spectra were identified using the 'findpeaks' function in MATLAB. The VSF was identified separately for each location within the flow field by the frequency of the largest peak in the power spectrum. These largest peaks were confirmed to be the VSF since they were consistent with the VSF_{exp} (±2 Hz). The VSF for the whole flow field was calculated as the mean VSF for all locations. The Strouhal number (St) was calculated according to the equation:

$$St = VSF \times D \times \mathbf{U}^{-1}. \quad (2)$$

To account for flow constriction near the cylinders due to solid blocking effects, we calculated St using the flow velocity:

$$\mathbf{U} = \mathbf{U_f} \times [W/(W - D)], \quad (3)$$

where U is the actual flow velocity in the region of the cylinder, U_f is the nominal flow velocity upstream of the cylinder, and W is the width of the working section of the flume. For all treatments and flow speeds, the strongest peak in power spectrum corresponded to the VSF. We used the power spectra to identify the regions of the flow field that were affected by the shedding of vortices. These regions were defined as locations exhibiting a peak in the frequency-power spectrum that exceeded our user-defined power threshold. The power threshold was determined separately for each flow speed and was calculated as 10% of the largest power magnitude detected in the flow field behind the single cylinder. Regions below this power threshold were considered to be unaffected by vortex shedding.

The strength and periodicity of the vortex streets were calculated from our frequency analyses. For each location in the flow field, the strength of the vortex street was calculated from the power spectrum as the area under the peak associated with the VSF. For this calculation, any peak in the power spectrum that exceeded the power threshold and exhibited a frequency that was less than 0.5 Hz different from the frequency of the highest peak was also included. We also calculated the periodicity of the vortex street, which was a measure of the 'noise' of the flow field. Periodicity was computed from the power spectrum as the ratio of the height (power) to width (frequency) for the peak associated with the VSF. A location with a high periodicity exhibited a peak with a large amplitude power that spanned a narrow range of frequencies.

To understand how the spacing of cylinders affected the spacing of vortices, we measured the wavelength of the vortex wake for all arrangements of cylinders and flow speeds. The wavelength of vortices in the wake was determined by the spatial wavelength of $\mathbf{U_y}$ along the axis extending behind the cylinders. The vortex wavelength was measured for each flow field time step using a fast Fourier transform of $\mathbf{U_y}$ versus position along the x-axis behind the trailing cylinder. The highest peak of the resultant power spectrum yielded the spatial frequency of vortices (vortices m^{-1}). The inverse of this frequency provided the instantaneous wake wavelength, which was then averaged for all time steps to produce the mean wavelength of the wake for the entire treatment.

Computational fluid dynamics

We modeled the two-dimensional flow fields around our tandem cylinder arrangements with computational fluid dynamics (CFD) to better understand how the spacing of cylinders affected the general patterns of vortex formation. This model numerically solved the Navier–Stokes equations that govern fluid motion under boundary conditions for a Newtonian and incompressible fluid. These simulations were performed with an in-house solver using a space–time finite element method (Tezduyar, 2003; Wang et al., 2010; Tian, 2014).

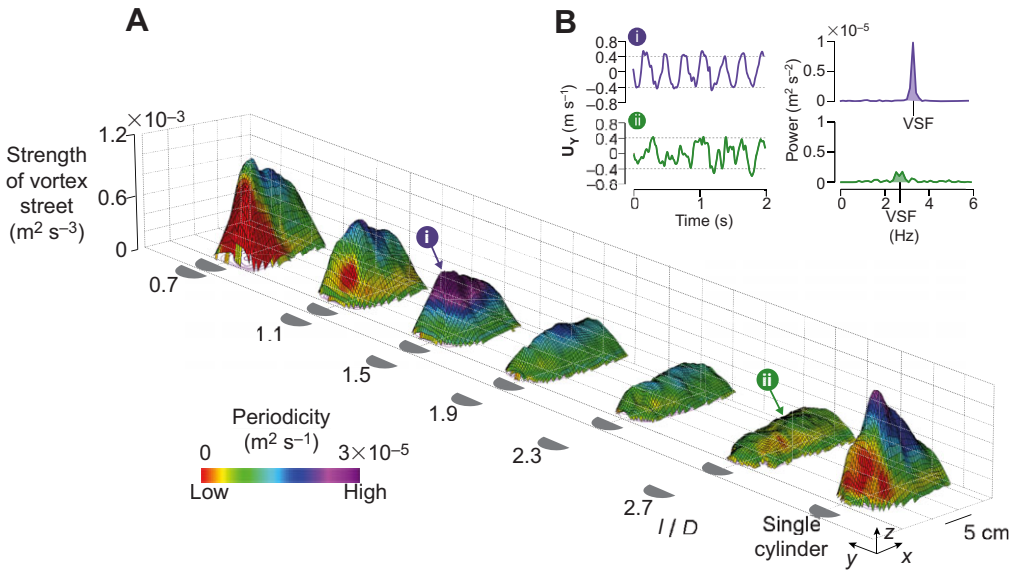

Fig. 3. Effect of cylinder spacing on the strength and periodicity of the vortex street behind tandem cylinders at *Re*=36,000. (A) Three-dimensional plots show the strength of the vortex street (*z*-axis) as a function of the spatial position behind the downstream cylinder (*x*–*y* axes), for each cylinder spacing arrangement. High periodicity (cool colors) indicates regions within the flow field that exhibit organized and stable vortices. Note that while the vortex strength generally declines as *l*/*D* increases from 0.7 to 2.7, some regions of high periodicity exist behind intermediate cylinder spacing conditions. (B) The lateral flow velocity ($\mathbf{U_y}$) over time and resultant power spectra for two locations in A (i and ii). The dominant peak in each power spectrum reveals the VSF. The size and shape of these peaks are used to calculate the vortex strength and periodicity for these specific locations. Specifically, vortex strength is calculated as the area under the peak associated with the VSF (shaded light purple and green), and periodicity is calculated as the height of this peak divided by its width. Note that (i) is a location that exhibits particularly strong and periodic vortices, as indicated by the large and narrow peak associated with the VSF. Data shown are from a representative flow speed of 0.7 m s^{-1} (*Re*=36,000).

Journal of Experimental Biology (2016) 219, 2182-2191 doi:10.1242/jeb.140475

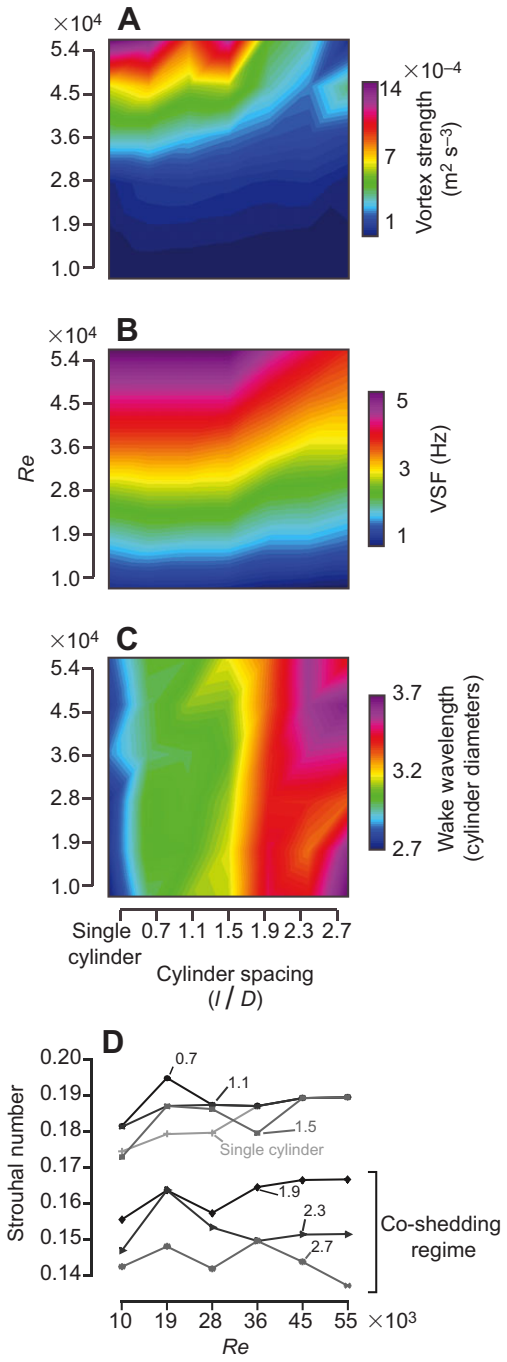

Fig. 4. Vortex street characteristics as a function of Reynolds number and cylinder spacing. (A) The strength of the vortex street decreases as the spacing of the cylinders increases, but increases within a given cylinder spacing as Reynolds number increases. (B) The VSF increases with Reynolds number. However, within a given Reynolds number, VSF actually decreases as cylinder spacing increases. (C) Cylinder wake wavelength increases with cylinder spacing for all Reynolds numbers. (D) The Strouhal number is higher for closely spaced cylinders than for widely spaced cylinders that operate within the co-shedding flow regime. Line labels indicate *l*/*D*.

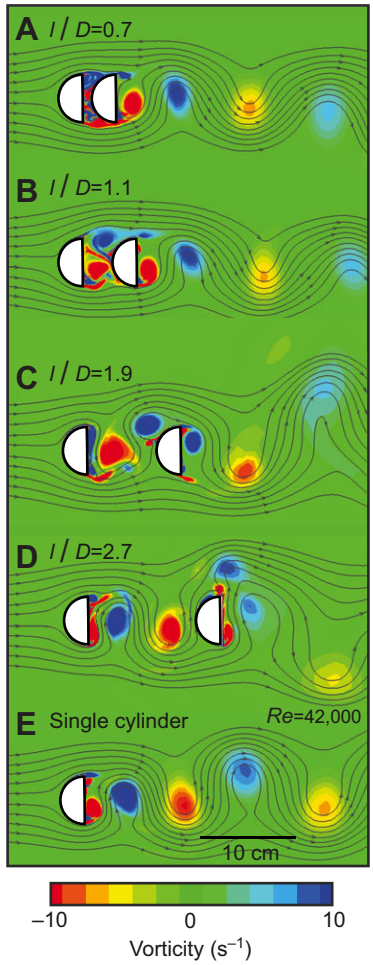

Fig. 5. Patterns of vortex formation around tandem cylinders. CFD modeling reveals vortex interactions between tandem cylinders create downstream vortex streets that differ from single cylinders. (A,B) The upstream cylinder of closely spaced cylinders generates attached vortices, resulting in a vortex street shed from the downstream cylinder that is similar to that of a single cylinder. (C,D) The upstream cylinder of widely spaced cylinders has room to generate a vortex street that interacts with the downstream cylinder. The complex interactions between upstream and downstream vortices cause the resultant vortex street to have a longer wake wavelength with weaker and less-organized vortices than when compared with a single cylinder situation. (E) von Kármán vortex street from a single cylinder is shown for reference. Data are shown for the representative flow speed of *Re*=42,000. Blue, clockwise rotation; red; counter-clockwise rotation. The streamlines are shown in gray.

The no-penetration and no-slip boundary conditions were prescribed at the cylinder surfaces. A velocity-inlet boundary condition was prescribed upstream of the cylinders and the traction free boundary condition was prescribed downstream of the cylinder wake. The remaining two outer boundary surfaces were prescribed with the far-field boundary condition. The inlet velocity was set equal to the nominal flow speeds used in our trout kinematics experiments. The computational domain surrounding the cylinders ($30D \times 12D$) was divided into 25,000 triangular elements with mesh spacing of $0.003D$ near the cylinders and a time step of $0.01D/U$ was used. Validations were performed to ensure numerical results presented here are independent of mesh size, time step and computational domain. Details of the CFD method used and its validations have been described previously (Wang et al., 2010; Tian, 2014).

RESULTS

The wake behind differently spaced tandem cylinders

Our DPIV analyses revealed that nearly all of our cylinder arrangements produced a coherent Kármán vortex street, which was characterized by the alternate formation and shedding of

Journal of Experimental Biology (2016) 219, 2182-2191 doi:10.1242/jeb.140475

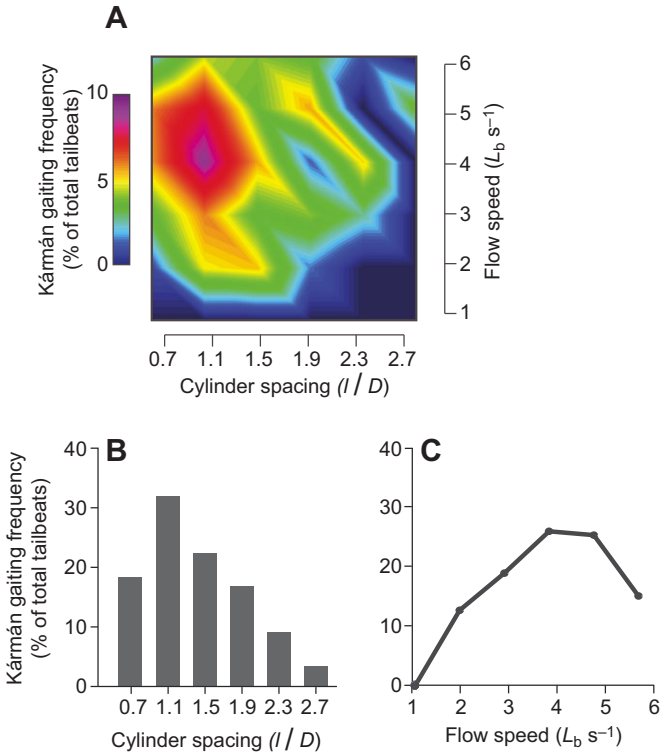

Fig. 6. Effect of cylinder spacing and flow speed on how often trout Kármán gaited. Intermediate cylinder spacings and flow speeds encourage Kármán-gaiting behavior. (A) Colors show the percentage of Kármán-gaiting tail beats observed as a function of cylinder spacing and flow speed. (B) The percentage of Kármán-gaiting tail beats when all flow speeds are pooled. (C) The percentage of Kármán-gaiting tail beats observed as a function of flow speed when all cylinder spacings are pooled.

counter-rotating vortices (Fig. 2). However, the structure of the downstream wake was strongly affected by the spacing between cylinders. For example, in comparison to a single cylinder, two closely spaced cylinders (*l*/*D*=0.7) reduced the area of the suction zone behind the downstream cylinder by over 50% (Fig. 2C). As the *l*/*D* ratio increased from 0.7 to 2.3, the vortices became spaced further apart (Fig. 2A) and exhibited smaller fluctuations in lateral velocity (Fig. 2B).

The strength of the vortices generally decreased as the spacing of cylinders increased. For example, at 4 L_b s^{-1} (*Re*=36,000), an increase in *l*/*D* from 0.7 to 2.7 caused an 83% attenuation in peak vortex strength, from 1.2×10^{-3} to 0.2×10^{-3} m^2 s^{-3} (Fig. 3). Similar trends occurred for all other flow speeds as *l*/*D* increased where, on average, there was a 72% decrease in peak vortex strength and a 53% decrease in average vortex strength across the entire flow field (Fig. 4A). In addition to these affects of cylinder spacing, we found that increasing the flow speed increased the vortex strength by at least an order of magnitude when *Re*=10,000–54,000. Therefore, cylinder spacing dictates vortex strength, which increases accordingly with flow speed.

Closely spaced cylinders produced regions within the wakes that were highly periodic, reflecting the presence of organized and stable vortices. For all flow speeds, the maximum periodicity measured behind the three most closely spaced cylinders was significantly greater than behind the three most widely-spaced arrangements (paired *t*-test, tstat=2.6, d.f.=5, *P*=0.05). It is important to note that the periodicity of the vortex street showed spatial variation within different regions of the wake, especially for the closely spaced cylinder arrangements (Fig. 3). Regions of low periodicity (warm colors in Fig. 3A) were located immediately behind the downstream cylinder or in the lateral regions of the vortex wake, while regions of high periodicity (cool colors in Fig. 3A) were located further downstream. Note that this variation in periodicity caused the average periodicity calculated over the entire wake to be indistinguishable between the closely and widely spaced cylinder arrangements for all speeds (paired *t*-test, tstat=1.6, d.f.=5, *P*=0.16).

The gap distance between two cylinders strongly affected the VSF and the spacing between successive vortices (i.e. wake wavelength). VSF increased with flow speed for all tandem cylinder treatments, similar to a single cylinder (Fig. 4B). Interestingly, we discovered that within a given flow speed, the VSF could decrease based solely on cylinder spacing once *l*/*D* exceeded 1.5. This meant that the VSF of widely spaced cylinders (*l*/*D*=2.7) was about 20% less than closely spaced cylinders (*l*/*D*=0.7). For perspective, in a single cylinder situation, such a change in VSF can only be achieved by reducing the flow speed by 20% (i.e. decreasing *Re* by about 5000 at this spatial scale). This change in VSF also decreased the Strouhal number (Fig. 4D). We found that the wake wavelength, which is set by the cylinder diameter in single cylinder situations irrespective of flow speed, actually increased when tandem cylinders were spaced further apart (Fig. 4C). Even at the closest cylinder spacing arrangement, the wake wavelength was longer than that of a single cylinder of the same diameter (15±0.2 cm vs 13.7±0.2 cm, mean±1 s.d.). As the gap between cylinders widened to an *l*/*D* of 2.7, the wake wavelength increased to 17.8±0.8 cm, which is ∼30% longer when compared with a single cylinder. As is the case for a single cylinder, changing the flow speed for a given cylinder spacing had little effect on the wake wavelength.

Computational simulations reveal how vortices form around tandem cylinders

We used CFD to simulate the flow around tandem cylinders in order to better understand how vortices are formed and shed under our experimental conditions (Fig. 5). Because our DPIV measurements were only focused on the downstream wake, the CFD simulations provided us with valuable insight into how the vortices created by the two cylinders interact to generate the resultant downstream vortex street. We compared the downstream flow fields predicted by CFD with those measured by DPIV and found agreement between the two. The CFD simulations showed that coherent vortices were shed by all cylinder arrangements across all flow speeds. Our DPIV measurements also indicated that coherent vortices were produced by the treatments, with the only exception being the widest cylinder arrangement at the highest *Re*. Our CFD simulations also predicted that the patterns of vortex formation depended strongly on *l*/*D*. When the distance between cylinders was small, vortices formed in the gap but usually stayed attached to the upstream cylinder (Fig. 5A). These gap vortices could also shed and combine with a vortex forming behind the downstream cylinder (Fig. 5B). The shear layer shed from the sides of the upstream cylinder appeared to reattach to the side of the downstream cylinder. When the distance between cylinders was *l*/*D*=1.9 or greater, vortices were shed from both upstream and downstream cylinders, where the upstream cylinder vortices combined in complex ways with vortices shed from the downstream cylinder (Fig. 5C,D). These complex vortex dynamics ultimately produced a less-organized vortex street behind the downstream cylinder.

Journal of Experimental Biology (2016) 219, 2182-2191 doi:10.1242/jeb.140475

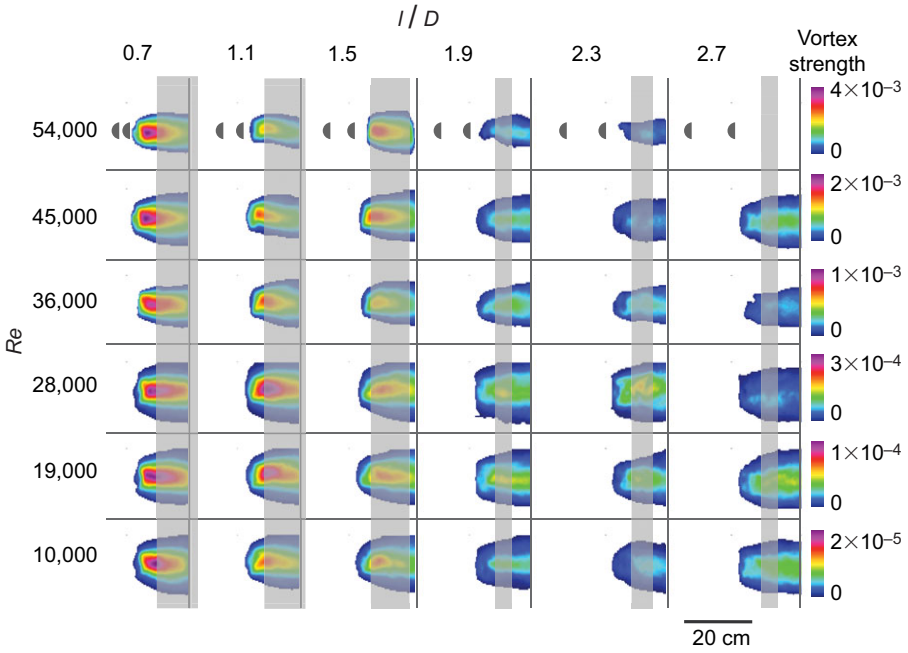

Fig. 7. The position of Kármán-gaiting trout within the vortex street behind tandem cylinders. Heat maps indicate vortex strength. White indicates regions that were unaffected by vortex shedding (see Materials and methods). Within a given flow speed, the area containing strong vortices (warm colors) decreases along with the peak vortex strength as cylinder spacing increases. Gray bars indicate the downstream position of a trout's rostrum when Kármán gaiting. The range of the gray bars corresponds to the 25th and 75th percentile of downstream positions measured for each cylinder spacing. Refuging trout show a more restricted range of downstream positions when cylinders are spaced further apart.

Trout Kármán gait more frequently behind closely spaced cylinder arrangements

For each trout, we recorded 10 min of swimming in each of our treatments and found that trout were able to Kármán gait behind all six tandem cylinders arrangements (l/D=0.7–2.7), but Kármán gaited more frequently behind closely spaced cylinders (Fig. 6A,B). Of all 222 Kármán-gaiting tail beats observed in the study, 73% occurred behind the three most closely spaced cylinder arrangements (l/D=0.7, 1.1, 1.5), while only 27% occurred behind the three most widely spaced cylinders (l/D=1.9, 2.3, 2.7). Only 4% of Kármán-gaiting tail beats occurred behind the most widely spaced cylinder arrangement (l/D=2.7). Flow speed also affected how often trout Kármán gaited. When results were pooled for all cylinder arrangements, we found that trout preferred intermediate flow speeds of 3–5 body lengths (L_b) per second for Kármán gaiting (Fig. 6C). Trout did not Kármán gait at all during the slowest flow speed of 1 L_b s^{-1}.

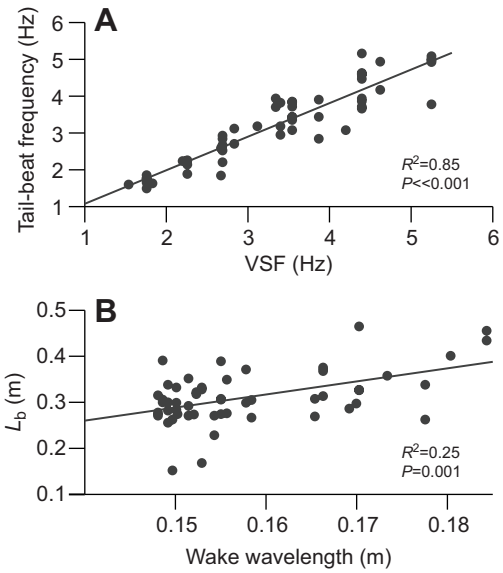

Fig. 8. The effect of vortex shedding frequency and wake wavelength on the kinematics of the Kármán gait. (A) Tail-beat frequency increases linearly with VSF (R^2=0.82, P<0.001). (B) Body wavelength increases with wake wavelength (e.g. vortex spacing, R^2=0.22, P=0.01).

Kármán gait kinematics in the vortex wake

We found that trout refuging behind tandem cylinders exhibited the hallmark characteristics of the Kármán gait (i.e. large-amplitude lateral motions of the body occurring at a low frequency) and the position where trout Kármán-gaited coincided with the stronger regions of the vortex wake (gray shaded regions in Fig. 7). When Kármán-gaiting behind closely spaced cylinders (l/D=0.7–1.1), trout positioned themselves along a wider range of downstream positions (~8–18 cm behind the downstream cylinder) because of the relatively larger region where the vortex street is strong (warm colors in Fig. 7). Trout refuging behind widely-spaced cylinders ($l/D\geq$1.9) were more spatially concentrated and restricted their position to ~8–13 cm behind the downstream cylinder. Again, this region where fish often refuged represents the strongest region of the vortex wake (Fig. 7).

The vortex wake also affected the tail-beat frequency and body wavelength of Kármán gaiting (Fig. 8). We found that the VSF explained 85% of the variation in tail-beat frequency for Kármán-gaiting trout (regression, P<0.001, R^2=0.85). We also found a significant linear relationship between the body wavelength and the wake wavelength, but this relationship only explained 25% of the variation in body wavelength (linear regression, P=0.001, R^2=0.25).

The spacing between tandem cylinders had only small effects on the Kármán-gait kinematics (Fig. 9). When the data were pooled across speeds, we found that increasing the cylinder spacing tended to increase the lateral motion of the head (regression, P=0.011, R^2=0.10) and the wavelength of the body (regression, P=0.004, R^2=0.15), and made the fish hold station closer to the downstream cylinder (regression, P=0.008, R^2=0.10). Note that there was a large variability associated with the kinematics, with the spacing of cylinders explaining less than 15% of the total variation for the parameters mentioned above. We also found that cylinder spacing did not affect the lateral amplitude of the tail (regression, P=0.61).

Journal of Experimental Biology

Journal of Experimental Biology (2016) 219, 2182-2191 doi:10.1242/jeb.140475

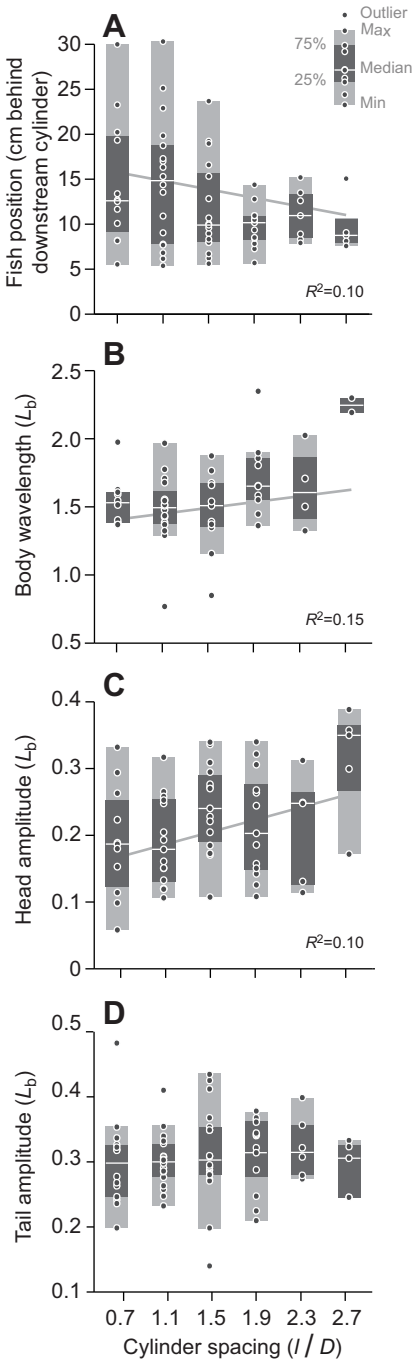

Fig. 9. Effect of cylinder spacing on the kinematics of the Kármán gait. Box and whisker plots show that cylinder spacing had small but significant effects on (A) the distance of the rostrum from the downstream cylinder (R^2=0.10, P=0.008), (B) body wavelength (R^2=0.15, P=0.004) and (C) lateral amplitude of the head (R^2=0.10, P=0.011) for data pooled across flow speeds. (D) Tail-beat amplitude does not change with increasing cylinder spacing (P=0.61).

DISCUSSION

In nature, interactions between flow and physical structures create microhabitats that fishes often exploit to save energy and acquire food resources (Liao, 2007). While lower flow velocities result from structures shielding the flow, it is becoming increasingly apparent that fishes are exploiting vortices to reduce the cost of locomotion (Przybilla et al., 2010; Liao et al., 2003b; Liao, 2004; Tritico and Cotel, 2010; Taguchi and Liao, 2011). Much of our understanding of how fishes exploit vortices has come from studies utilizing single-cylinder experiments. Yet the hallmark of natural, lotic environments is their structural and hydrodynamic complexity (Roper et al., 1998; Tritico and Hotchkiss, 2005). To begin to dissect how fish relate to more complex flows shed by aggregations of structures, we investigated here the ability of trout to refuge behind two cylinders in flow. Our findings are summarized in Fig. 10. We show that the vortex wakes behind tandem cylinders are substantially different from those behind a single cylinder, yet all of these wakes can be exploited by Kármán-gaiting trout. However, only specific combinations of flow velocity and cylinder spacing are most conducive for Kármán gaiting. For example, trout do not Kármán gait when the flow is less than 2 L_b s^{-1} and rarely Kármán gait when cylinders are spaced widely apart. Overall, trout prefer the strong and organized vortices shed by closely spaced, tandem cylinders, which is the wake most similar to that of a single cylinder.

Kármán gaiting is discouraged by the co-shedding regime and fast flow

Trout Kármán gait most often in the wake behind two cylinders positioned closely together. This is because closely spaced cylinders form strong and organized vortices, through the extended body and reattachment flow regimes, that drive the Kármán gait (Fig. 10A). Specifically, the fish experiences lift and thrust as the high-speed lateral flows associated with these vortices interact with the body of the animal (Liao et al., 2003a). In contrast, trout only rarely Kármán gait during the co-shedding regime because they encounter weak vortices at relatively low frequencies (Fig. 10B). Because Kármán gaiting depends on lift and thrust generated by the interaction of vortices and a compliant body, weaker vortices result in decreased opportunities to exploit the energy of the wake and result in overall lower propulsion. The wider spacing of vortices behind co-shedding cylinders only amplifies this effect because it causes the animal to encounter fewer vortices over time. In addition, the co-shedding regime produces a wake that is less periodic and less organized than the other flow regimes of tandem cylinders, where chaotic flows can punctuate otherwise periodic vortex streets (Igarashi, 1981). This may prove to be essential for fish to sustain Kármán gaiting. Indeed, trout only Kármán gaited for very brief periods during the co-shedding regime, which likely corresponded to when vortices were most predictable (e.g. the last 0.5 s of the green trace in Fig. 3B). Even if an obstacle is the appropriate size for Kármán gaiting (l:D=2–4:1, Akanyeti and Liao, 2013a,b), when two obstacles are found in tandem, trout are unlikely to refuge if the co-shedding regime is established. For tandem D-cylinders, this will typically occur when l/D exceeds 1.5.

Trout Kármán gaited the most behind tandem cylinders at intermediate flow speeds, similar to trout refuging behind a single cylinder (Akanyeti and Liao, 2013a). This is because at very low flow speeds the vortex street is not adequately developed enough for fish to exploit the vortices. When very high flow speeds are approached, the wake becomes increasingly unstable and complex (Wei and Smith, 1986), which in this study is likely to be reflected as the fewer occurrences of Kármán gaiting at the highest flow speed of 6 L_b s^{-1}.

Cylinder gap distance dictates vortex spacing and strength

In our study, widely spaced cylinders shed vortices that are spaced further apart than more closely spaced cylinders. These findings depart from the hydrodynamics of a single cylinder, where the

Journal of Experimental Biology (2016) 219, 2182-2191 doi:10.1242/jeb.140475

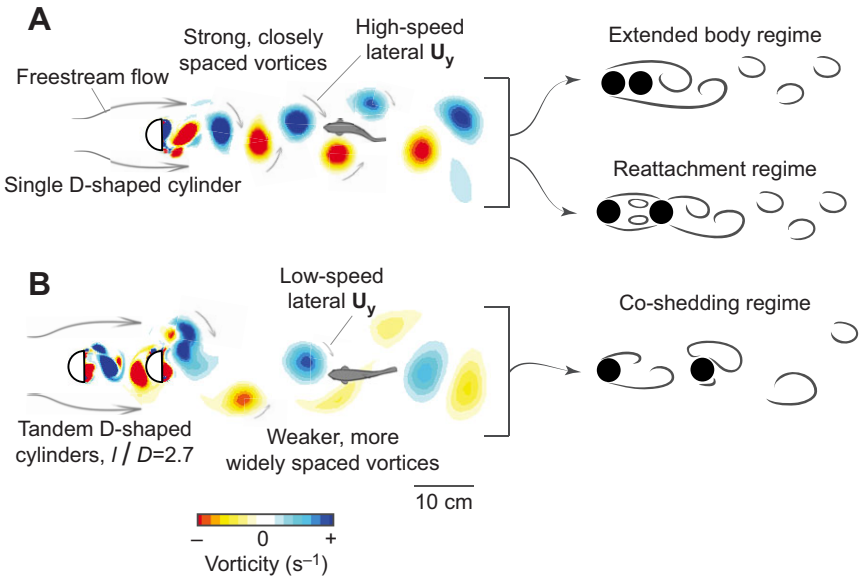

Fig. 10. The hydrodynamic regimes that encourage Kármán gaiting in trout. (A) Trout Kármán gait during the extended body and reattachment flow regimes produced by closely spaced cylinders due to the presence of strong, periodic vortices, similar to the vortex street behind a single cylinder. (B) Trout rarely Kármán gait in the co-shedding regime produced by widely spaced cylinders because the vortices are comparatively weaker, less predictable and more distantly spaced. Gray arrows illustrate the general direction and speed of flow near the shed vortices. Color shows the patterns of vortex formation revealed from CFD simulations. Blue, clockwise rotation; red, counter-clockwise rotation. Schematics in the right column are adapted from Igarashi (1981).

spacing of vortices (i.e. wake wavelength) is dictated only by the diameter of the cylinder according to the Strouhal equation (Zdravkovich, 1997; Liao et al., 2003a). We discovered that if the spacing between tandem cylinders is large enough it can lengthen the wake wavelength. The increase in wake wavelength is driven by two factors that arise from the complex interaction of flow between the leading and trailing cylinders. First, flow velocity is relatively high behind the trailing cylinder as a result of the reduced size of the suction zone. This region of faster flow translates each shed vortex from the trailing cylinder more quickly downstream than would otherwise be possible with a single cylinder. It is this faster flow in the tandem cylinder situation that likely increases the spacing between each successive vortex in the downstream wake. Second, the complex interactions of vortices unique to the co-shedding regime cause the VSF to decrease, which further increases the distance between shed vortices (Fig. 10). This is also indicated by a decreased Strouhal number (Strouhal number is typically constant for a single bluff body), which we found when l/D exceeded 1.5 (Fig. 4D) and the co-shedding regime became established. This effect is so pronounced that co-shedding tandem cylinders may shed vortices at a similar rate as a single cylinder that is ∼30% larger in diameter. However, it should be noted that the vortices shed by tandem cylinders in this situation would be considerably weaker and less organized that those shed by the larger single cylinder. Nonetheless, we show here that simply increasing the spacing between tandem D-cylinders changes the wake wavelength. This phenomenon has interesting experimental applications, such as the ability to independently test the effect of vortex size on Kármán gaiting separately from vortex spacing, which is impossible to do with single cylinders (Liao et al., 2003a).

Tandem cylinders to study fish sensory-motor integration in turbulent flows

The complex wakes produced by tandem cylinders in flow may prove useful in understanding the sensory-motor integration of refuging fish. Previous work has mainly concentrated on understanding the kinematics of refuging in fish, but we know little about how fish use different sensory systems to identify and exploit structures in flow. We have previously found that vision and the flow-sensitive lateral line system both play roles in refuging, yet fish are able to Kármán gait behind a single cylinder when only one of these modalities (i.e. vision or lateral line) is operational (Liao, 2006). This is probably because, in a single cylinder situation, the visual and hydrodynamic cues are closely correlated and predictable because of the stable characteristics of the vortex wake. However, do the respective roles of vision and flow sensing change when fish refuge behind aggregations of structures in flow? We suggest that tandem cylinders provide unique opportunities to address these types of questions. Very subtle changes in the position of cylinders can produce dramatic changes in the flow field. Therefore, visual and hydrodynamic stimuli are not closely correlated. By manipulating the structure of the vortex wake with small changes in the arrangement of the cylinders, it is possible to evaluate the roles of different sensory systems because hydrodynamic stimuli are drastically altered whereas visual cues remain effectively constant. Such independent control over visual and hydrodynamic cues may yield insight into how fish integrate different sensory modalities while refuging.

Object shape affects the establishment of hydrodynamic regimes

We found that for tandem objects, shape can impact the downstream flow such that it can actually delay the establishment of hydrodynamic regimes. Tandem D-shaped cylinders form vortices in patterns that are distinct from those reported for tandem whole cylinders at similar Reynolds numbers. For example, closely spaced whole cylinders establish an extended body regime (Lin et al., 2002; Igarashi, 1981), while we found that similarly spaced D-shaped cylinders do not. Instead, vortices form between D-shaped cylinders, setting up a reattachment regime. Tandem D-shaped cylinders also produce a co-shedding regime at much shorter gap distances (l/D>1.5) when compared with whole cylinders (l/D> ∼3, Igarashi, 1981; Sumner, 2010). This indicates that not only is gap spacing important for structures in current-swept environments, but their shape can also play a crucial role in downstream wake dynamics. This leads us to predict that fish in the field will Kármán gait behind objects of a certain shape and not others, even if the spacing is identical.

Tandem cylinders elicit variable Kármán-gait kinematics

We found that the kinematics of Kármán gaiting varied more behind tandem cylinders than behind single cylinders (Akanyeti

and Liao, 2013a). This indicates that fish employ a greater diversity of swimming motions when Kármán gaiting, which may include corrective motions. For example, one standard deviation for kinematic parameters behind tandem cylinders (the lateral amplitude of the head and tail and the wavelength of the body) was greater (35.3%, 18.0% and 14.6% of the mean, respectively) than for the same parameters behind a single cylinder (13% or less of the mean; Akanyeti and Liao, 2013a). In addition, body wavelength exhibited a wide range of values for fish refuging behind tandem cylinders (0.75–2.3 L_b, Fig. 8). When comparing the body wavelengths of fish from the present study at *Re*=28,000 to similarly sized fish refuging behind a single cylinder at similar *Re* (Akanyeti and Liao, 2013a), we found that body wavelength was slightly longer and more variable behind tandem cylinders (1.65±0.26 L_b) versus a single cylinder (1.52±0.12 L_b).

We propose two possible explanations for the higher variation in kinematics behind tandem cylinders. First, the wake may not dictate the posture of the body as extensively as when Kármán gaiting behind a single cylinder, and fish may be able to exploit vortices by employing a greater range of motions than previously described (Liao et al., 2003a). Whether these motions of the body are under active control, or are the result of passive fluid–structure interactions, remains to be determined. Second, fish motions may be tightly locked to the wake, but the large variability of the wake makes it so that the kinematics also show great variability. This is a likely scenario for unstable wakes behind widely spaced cylinders, where successively shed vortices tend to vary in strength and size (Sumner, 2010). In this way, the variability in kinematics reflects the dynamic nature of the wakes behind tandem cylinders. These results reveal that fish may possess more flexibility in Kármán gait kinematics than previously thought.

One major similarity between Kármán gaiting behind single and tandem cylinders is that the VSF is a strong predictor of the tail-beat frequency (Fig. 8A). This suggests that in order to Kármán gait, fish must be certain that each shed vortex interacts with its body. It is likely that a fish may make small alterations in its motion and posture, which would contribute to the high variation in kinematics discussed above, but still must tightly synchronize the timing of swimming with the passing vortices in order to Kármán gait.

Understanding the hydrodynamic mechanisms underlying when and where fish refuge behind multiple objects is challenging, but has many applications across the fields of fisheries science, ecology and fluid dynamics. Here, we have demonstrated that fish selectively refuge behind a simple arrangement of two cylinders, but the ability to refuge behind more complex arrangements of objects remains entirely unexplored. We believe that this is a promising step for future investigations and may substantially advance our understanding of how fish spatially distribute themselves in natural habitats.

Acknowledgements
We would like to thank J. Johansen for helpful discussions about this project and A. Peterson for assistance with fish care.

Competing interests
The authors declare no competing or financial interests.

Author contributions
J.C.L. designed the study. J.C.L and C.J.W. conducted the swimming kinematics experiments. W.J.S. and O.A. conducted the particle image velocimetry experiments. F.-b.T. developed the model and performed the flow simulations. W.J.S. performed the data analysis. W.J.S., J.C.L. and O.A. interpreted the data. W.J.S. and J.C.L. wrote the manuscript.

Funding
This work was supported by the National Institutes of Health [RO1 DC010809] and the National Science Foundation [IOS-1257150 to J.C.L.]

References
Akanyeti, O. and Liao, J. C. (2013a). The effect of flow speed and body size on Kármán gait kinematics in rainbow trout. *J. Exp. Biol.* **216**, 3442-3449.
Akanyeti, O. and Liao, J. C. (2013b). A kinematic model of Kármán gaiting in rainbow trout. *J. Exp. Biol.* **216**, 4666-4677.
Blevins, R. D. (1990). *Flow Induced Vibration*. Malabar, FL: Krieger Publishing Company.
Enders, E. C., Boisclair, D. and Roy, A. G. (2003). The effect of turbulence on the cost of swimming for juvenile Atlantic salmon (*Salmo salar*). *Can. J. Fish. Aquat. Sci.* **60**, 1149-1160.
Igarashi, T. (1981). Characteristics of the flow around two circular cylinders arranged in tandem: 1st report. *Bull. JSME* **24**, 323-331.
Liao, J. C. (2004). Neuromuscular control of trout swimming in a vortex street: implications for energy economy during the Kármán gait. *J. Exp. Biol.* **207**, 3495-3506.
Liao, J. C. (2006). The role of the lateral line and vision on body kinematics and hydrodynamic preference of rainbow trout in turbulent flow. *J. Exp. Biol.* **209**, 4077-4090.
Liao, J. C. (2007). A review of fish swimming mechanics and behaviour in altered flows. *Philos. Trans. R. Soc. B Biol. Sci.* **362**, 1973-1993.
Liao, J. C., Beal, D. N., Lauder, G. V. and Triantafyllou, M. S. (2003a). Fish exploiting vortices decrease muscle activity. *Science* **302**, 1566-1569.
Liao, J. C., Beal, D. N., Lauder, G. V. and Triantafyllou, M. S. (2003b). The Kármán gait: novel body kinematics of rainbow trout swimming in a vortex street. *J. Exp. Biol.* **206**, 1059-1073.
Lin, J.-C., Yang, Y. and Rockwell, D. (2002). Flow past two cylinders in tandem: instantaneous and averaged flow structure. *J. Fluid Struct.* **16**, 1059-1071.
McLaughlin, R. L. and Noakes, D. L. (1998). Going against the flow: an examination of the propulsive movements made by young brook trout in streams. *Can. J. Fish. Aquat. Sci.* **55**, 853-860.
Przybilla, A., Kunze, S., Rudert, A., Bleckmann, H. and Brücker, C. (2010). Entraining in trout: a behavioural and hydrodynamic analysis. *J. Exp. Biol.* **213**, 2976-2986.
Roper, B. B., Konnoff, D., Heller, D. and Wieman, K. (1998). Durability of Pacific Northwest instream structures following floods. *N. Am. J. Fish. Manage* **18**, 686-693.
Sumner, D. (2010). Two circular cylinders in cross-flow: a review. *J. Fluid Struct.* **26**, 849-899.
Taguchi, M. and Liao, J. C. (2011). Rainbow trout consume less oxygen in turbulence: the energetics of swimming behaviors at different speeds. *J. Exp. Biol.* **214**, 1428-1436.
Tezduyar, T. E. (2003). Computation of moving boundaries and interfaces and stabilization parameters. *Int. J. Numer. Methods Fluids* **43**, 555-575.
Tian, F.-B. (2014). Deforming-spatial-domain/stabilized space-time (DSD/SST) method in computation of non-Newtonian fluid flow and heat transfer with moving boundaries. *Comput. Mech.* **54**, 581-589.
Tritico, H. M. and Cotel, A. J. (2010). The effects of turbulent eddies on the stability and critical swimming speed of creek chub (*Semotilus atromaculatus*). *J. Exp. Biol.* **213**, 2284-2293.
Tritico, H. M. and Hotchkiss, R. H. (2005). Unobstructed and obstructed turbulent flow in gravel bed rivers. *J. Hydraul. Eng.* **131**, 635-645.
Wang, S.-Y., Tian, F.-B., Jia, L.-B., Lu, X.-Y. and Yin, X.-Z. (2010). secondary vortex street in the wake of two tandem circular cylinders at low Reynolds number. *Phys. Rev. E* **81**, 036305.
Webb, P. W. (1998). Entrainment by river chub *Nocomis micropogon* and smallmouth bass *Micropterus dolomieu* on cylinders. *J. Exp. Biol.* **201**, 2403-2412.
Wei, T. and Smith, C. R. (1986). Secondary vortices in the wake of circular cylinders. *J. Fluid Mech.* **169**, 513-533.
Xu, G. and Zhou, Y. (2004). Strouhal numbers in the wake of two inline cylinders. *Exp. Fluids* **37**, 248-256.
Zdravkovich, M. M. (1997). *Flow Around Circular Cylinders: A Comprehensive Guide Through Flow Phenomena, Experiments, Applications, Mathematical Models, and Computer Simulations*. Oxford, UK: Oxford Science Publications, Oxford University Press.